Praise Worthy Prize

This paper is available online at www.praiseworthyprize.org
International Review on Modelling and Simulations (I.RE.MO.S.), Vol. 12, N. 1
ISSN 1974-9821 *February 2019*

Precursors of Instability for a Vehicle Traveling in Curve

Giandomenico Di Massa, Sebastian Rosario Pastore, Riccardo Russo, Francesco Timpone

Abstract - *Nowadays, the automotive field takes care of human safety in the everyday driving. In this sense, the vehicle dynamics control systems and ADAS (Advanced Driver Assistance System) play a crucial role for both active and passive safety. In terms of handling, the critical issues for the everyday driver are during braking or steering maneuvers: the main idea of this paper is to investigate the possibility to recognize some critical behaviors leading to vehicle instability, using only the wheel sensors signals, already available as mandatory in actual passenger car (in particular for ABS). In order to do this, a seven degrees of freedom model of a vehicle that runs in a curve with constant longitudinal speed is formulated. With no particular reference to the power unit (IC motor or electrical motors), three different traction schemes configurations are considered. The numerical solutions of the model are analyzed to evaluate their stability, the associated modal shapes and the modal participation factors. A systematic analysis allows recognizing some vehicle behaviors that may constitute instability precursors useful to develop a suitable control logic. Results provided by both a standard vehicle dynamics simulation software and a "on-road" test are presented and discussed to verify the actual feasibility of the proposed precursors employment.* ***Copyright © 2019 The Authors.***

Keywords*: Precursors, Instability, Vehicle Dynamics, Curve Traveling*

Nomenclature

A	Vehicle front section (m^2)
a	Vehicle CoG - front axle distance (m)
A_y	Lateral acceleration (ms^{-2})
b	Vehicle CoG - rear axle distance (m)
C_x	Aerodynamic drag coefficient
d	Roll center height (m)
F_{xij}, F_{yij}, F_{zij}	Road-Tire force components (N) (i=1,2; j=1,2)
GXY	Reference frame fixed to the vehicle body with origin in the Center of Gravity
g	Gravity (ms^{-2})
h	CoG height (m)
J_r	Tire mass moment of inertia around the rotation axis (kgm^2)
J_z	Vehicle mass moment of inertia around vertical axis
K_1	Front roll stiffness (Nm)
K_2	Rear roll stiffness (Nm)
m	Vehicle mass (kg)
M_{ij}	Torque on the tires (Nm)
$P_{Coefficient}$	Coefficients in the Pacejika magic formula
Q, P	Right and left eigenvectors matrix
R	Curve radius (m)
R_0	Tire rolling radius
r	Yaw rate (s^{-1})
s_{ij}	Tires longitudinal slip
t	Tread (m)
U	Longitudinal velocity (ms^{-1})
V	Lateral velocity (ms^{-1})
α_{ij}	Tires lateral slip
λ_k	Eigenvalues (k= 1,7)
ρ	Air density (kgm^{-3})
ρ_{ij}	Modal participation factors
β	Side slip angle
δ	Front wheel angle
ω_{ij}	Tires angular velocity (s^{-1})

I. Introduction

In order to improve vehicle and pedestrian safety, modern cars are equipped with sophisticated control systems, which assist the driver in potentially dangerous situations [1]. Some of these control systems act on brakes and engine based on signals coming out from tires, vehicle body and engine. More complex control systems, such as Advanced Driver Assistance Devices (ADAS), also act on other devices such as differentials, steering and suspensions based on additional signals coming out from GPS, vision systems, radars and, eventually, from other vehicles. Travelling a curve, a vehicle can be seen as a combination of a number of nonlinear subsystems [2], [3] interacting with the road by means of the four tires in different conditions (depending on tire pressure, tire temperature, icy, wet, and dry road, etc.) the forces deriving from such interactions are

Available online by February 28th, 2019 https://doi.org/10.15866/iremos.v12i1.16902

described in literature by empirical models [4] fitted with a number of parameters affected by great uncertainty.

Therefore, a complete and reliable description of the vehicle dynamics behavior constitutes a very complex problem from both the mathematical and the numerical point of view. In general, a control logic has a great number of reliable signals, but, in order to perform its tasks in a few milliseconds, must fix the reference values for the controlled variables [5] adopting either: control maps or very light and simplified reference models. In the last years, a great number of papers, dealing with control logic developments, have been published in the specific literature [6]. With reference to vehicle dynamics control logics, typically, the reference values are fixed based on linearized models [7], simplified bicycle models [8], [9] or static control maps [10]. The cited papers represent only an example of a general tendency common to the whole, very wide, literature on this matter. Due to fuzzy definition of some reference models, control logics must act softly and, above all, only if it is strictly necessary. Therefore, in their development, it is very important to set suitable and reliable thresholds of activation [1], [11] based on signals that may be considered precursors of dangerous situations. The present paper deals with the study of the in-curve motion lateral stability of a vehicle. The aim is to find some instability precursors in the signals coming out from the sensors equipping the car. In particular in this paper the attention is focused on the four tire encoder signals. In fact, such encoders are mandatory present on all modern cars, being components of the ABS control system. The instability precursors could be of course found also in other sensors signals, such as yaw rate sensors, accelerometers, and other measurement devices equipping the car.

To this purpose, the classical seven degrees of freedom model of the vehicle is employed accounting for the in-plane car motions and the four tire rotations, moreover the tire-road interaction is modeled by the Pacejka magic formula. With no particular reference to the power unit (IC motor or electrical motors), three different traction schemes configurations have been considered: Rear Drive (RWD), Front Drive (FWD) and Four-Wheel Drive (4WD). In all the cases studied in this paper, only open differentials have been employed, but the described approach is suitable for any torque repartition logic [12], [13]. By using such classical model of vehicle, it is possible to find the steady state conditions characterizing the in-curve motion of a car with constant longitudinal speed. Such steady state conditions are the equilibrium points for the nonlinear motion equations system. After linearization in the range of the equilibrium point, by means of the classical linear stability analysis instruments, it is possible to investigate about eigenvalues, modal shapes and participation factors looking for events that, occurring always in proximity of instability, may be considered as its "precursors". The idea to investigate on the modal shapes is not new in the motorcycle field of application [14], while it is not so used in the vehicles dynamics ambit. Therefore, in order to verify the feasibility of the proposed precursors employment, the output provided by both a standard simulation software and an on-road test will be presented and discussed.

II. The Mathematical Model

This study deals with the motion stability analysis of a vehicle moving in a curve with constant longitudinal velocity. Three kinds of powertrains (Rear, Front, Four Wheel drive) have been considered. The goal is to highlight the different behaviors characterizing the vehicle's motions in proximity of the instability threshold with the aim to find some "instability precursors" useful to activate suitable Vehicle Dynamics Control strategies.

The vehicle dynamics is described by a classical 7 degrees of freedom quadricycle planar model. Fig. 1 represents the reference frame GXY, fixed to the car body with the origin in the vehicle center of mass G, the axes X and Y are directed along the longitudinal and transversal car axes. In such reference frame the absolute vehicle velocity and its yaw rate are indicated with v and r respectively.

The longitudinal and transversal velocities (i.e. the components of v along X and Y axes) are indicated with U and V respectively. The vehicle dynamics can be described by the following set of seven nonlinear first order differential equations [2], [3]:

$$\begin{aligned}
\dot{U} = {} & Vr + \frac{1}{m}\Big[F_{x21} + F_{x22} - \left(F_{y11} + F_{y12}\right)\sin(\delta) + \\
& + \left(F_{x11} + F_{x12}\right)\cos(\delta) - \frac{\rho A C_x U^2}{2}\Big] \\
\dot{V} = {} & -Ur + \frac{1}{m}\Big[\left(F_{y11} + F_{y12}\right)\cos(\delta) + \\
& + \left(F_{x11} + F_{x12}\right)\sin(\delta) + \left(F_{y21} + F_{y22}\right)\Big] \\
\dot{r} = {} & \frac{1}{J_z}\Big[a\left(F_{y11} + F_{y12}\right)\cos(\delta) + \\
& + a\left(F_{x11} + F_{x12}\right)\sin(\delta) - b\left(F_{y21} + F_{y22}\right) + \\
& - \frac{t}{2}\left(F_{x21} - F_{x22}\right) - \frac{t}{2}\left(F_{x11} - F_{x12}\right)\cos(\delta) + \\
& + \frac{t}{2}\left(F_{y11} - F_{y12}\right)\sin(\delta)\Big] \\
\dot{\omega}_{ij} = {} & \frac{\left(M_{ij} - F_{xij} R_0\right)}{J_r} \quad i = 1,2;\ j = 1,2
\end{aligned} \tag{1}$$

in which the known parameters are m, J_z, J_r, a, b, t, h, d, g, ρ, A, C_x, K_1, K_2, $P_{Coefficient}$, constituted by the vehicle's inertial and geometrical characteristics, the aerodynamic parameters, the suspension stiffnesses and the Pacejka magic formula coefficients the last two used to evaluate the forces in (1) as shown below: the five input

parameters, characterizing the maneuver, are the driving torque on each tire (depending on the adopted traction scheme) and the wheel steering angle:

$$M_{11}, M_{12}, M_{21}, M_{22}, \delta$$

The eight force components F_{xij} and F_{yij} are all evaluated by means of the combined Pacejka magic formula [4]:

$$F_{kij} = Pacejka\left(F_{zij}, \alpha_{ij}, s_{ij}; P_{Coefficients}\right),$$
$$k = x, y;\ i = 1, 2;\ j = 1, 2$$

where the state dependent terms F_{zij}, α_{ij} and s_{ij} are evaluated in accordance with the classical formulas:

$$\begin{aligned}
F_{z11} &= -\frac{mg}{2}\frac{b}{a+b} + \frac{d}{t}m\frac{b}{a+b}Ur + \\
&+ \frac{K_1}{K_1+K_2}m\frac{h-d}{t}Ur \\
F_{z12} &= -\frac{mg}{2}\frac{b}{a+b} - \frac{d}{t}m\frac{b}{a+b}Ur + \\
&- \frac{K_1}{K_1+K_2}m\frac{h-d}{t}Ur \\
F_{z21} &= -\frac{mg}{2}\frac{a}{a+b} + \frac{d}{t}m\frac{a}{a+b}Ur + \\
&+ \frac{K_2}{K_1+K_2}m\frac{h-d}{t}Ur \\
F_{z21} &= -\frac{mg}{2}\frac{a}{a+b} - \frac{d}{t}m\frac{a}{a+b}Ur + \\
&- \frac{K_2}{K_1+K_2}m\frac{h-d}{t}Ur \\
\alpha_{11} &= \delta - \frac{V+ra}{U-r\frac{t}{2}};\ \alpha_{12} = \delta - \frac{V+ra}{U+r\frac{t}{2}}; \\
\alpha_{21} &= -\frac{V+rb}{U-r\frac{t}{2}};\ \alpha_{22} = -\frac{V+rb}{U-r\frac{t}{2}} \\
s_{11} &= \frac{\omega_{11} - \frac{U-r\frac{t}{2}}{R_0}\cos\delta}{\frac{U-r\frac{t}{2}}{R_0}\cos\delta};\ s_{12} = \frac{\omega_{12} - \frac{U+r\frac{t}{2}}{R_0}\cos\delta}{\frac{U+r\frac{t}{2}}{R_0}\cos\delta}; \\
s_{21} &= \frac{\omega_{21} - \frac{U-r\frac{t}{2}}{R_0}}{\frac{U-r\frac{t}{2}}{R_0}};\ s_{22} = \frac{\omega_{22} - \frac{U+r\frac{t}{2}}{R_0}}{\frac{U+r\frac{t}{2}}{R_0}}
\end{aligned} \tag{2}$$

The above system of equations has been used to describe the dynamical behavior of a vehicle running a curve with constant engine power and wheel angle. Sudden variations in power and steering will involve other dynamic phenomena, such as dynamic load transfer, lag in the tires, transversal aerodynamic forces, spinning and etc., whose study is far from the aims of this paper. For the above reasons the described model is valid only in the neighborhood of a steady state solution $\bar{S} = \left\{\bar{U}, \bar{r}\ , \bar{V}, \bar{\omega}_{11}, \bar{\omega}_{12}, \bar{\omega}_{21}, \bar{\omega}_{22}\right\}$.

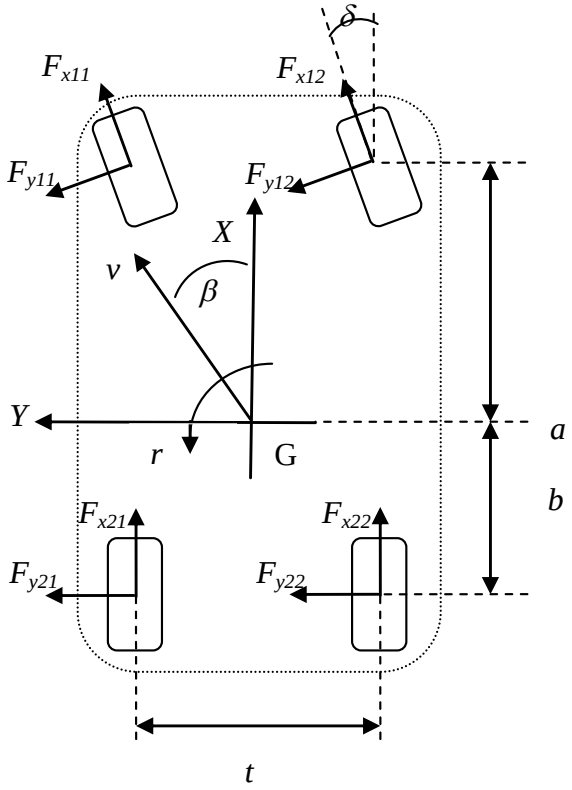

Fig. 1. Schematic for the mathematical system

II.1. Steady State Solution and Stability Analysis

Three different traction schemes have been considered: rear wheel drive (RWD), front wheel drive (FWD) and four-wheel drive (4WD). In RWD and FWD schemes it has been supposed the presence of an open differential splitting the engine torque, M, into two equal quantities between the two driving wheels. In 4WD case it has been supposed the presence of three open differentials splitting the engine torque, *M*, a quarter for each driving wheel. In order to find the above-mentioned steady state solutions in a systematic way, a recursive procedure has been adopted, as described below. Once fixed the desired curve radius *R* and the vehicle traction scheme configuration, the total engine torque has been varied starting from 5 Nm to each total engine torque, with an incremental step of 5 Nm. To run the desired curve, the wheel angle $\bar{\delta}$ has been found together with the steady state solution $\bar{S}$ by solving a set of eight algebraic nonlinear equations:

$$
\begin{aligned}
0 &= Vr + \frac{1}{m}\Big[F_{x21} + F_{x22} - \left(F_{y11} + F_{y12}\right)\sin(\delta) + \\
&+ \left(F_{x11} + F_{x12}\right)\cos(\delta) - \frac{\rho A C_x U^2}{2}\Big] \\
0 &= -Ur + \frac{1}{m}\Big[\left(F_{y11} + F_{y12}\right)\cos(\delta) + \\
&+ \left(F_{x11} + F_{x12}\right)\sin(\delta) + \left(F_{y21} + F_{y22}\right)\Big] \\
0 &= \frac{1}{J_z}\Big[a\left(F_{y11} + F_{y12}\right)\cos(\delta) + \\
&+ a\left(F_{x11} + F_{x12}\right)\sin(\delta) + \\
&- b\left(F_{y21} + F_{y22}\right) - \frac{t}{2}\left(F_{x21} - F_{x22}\right) + \\
&- \frac{t}{2}\left(F_{x11} - F_{x12}\right)\cos(\delta) + \\
&+ \frac{t}{2}\left(F_{y11} - F_{y12}\right)\sin(\delta)\Big] \\
0 &= \frac{\left(M_{ij} - F_{xij} R_0\right)}{J_r} \quad i = 1,2;\ j = 1,2 \\
0 &= R - \sqrt{\left(\frac{V}{r}\right)^2 + \left(\frac{U}{r}\right)^2}
\end{aligned}
\tag{3}
$$

At each step the algebraic system is solved numerically by adopting the solution of the previous step as initial condition (for the first step a set of "quasi zeros" initial condition values is used). For each numerical solution $\left[\bar{S}, \bar{\delta}\right]$ the Jacobian matrix is computed. The upper left [7×7] submatrix of such Jacobian matrix coincides with the linearized motion equation State Matrix (1). It is then possible to evaluate the eigenvalues vector λ_k and the right eigenvectors matrix [Q]. For the found solution stability all the real parts of the seven eigenvalues of the linearized state matrix must be negative. This described recursive procedure is repeated until the first unstable solution is found (i.e. until the real part of one of the seven state matrix eigenvalues becomes not negative). For each steady state solution, it is possible to evaluate:

$$\beta = \tan^{-1}\left(\frac{V}{U}\right)$$

and:

$$A_y = Ur$$

In this way, the classical β vs r and δ vs A_y curves may by plotted. Moreover, once given the right eigenvectors matrix [Q] and its left counterpart $\left[P\right] = \left[Q^{-1}\right]^T$, it is possible to evaluate the participation factors:

$$\rho_{jk} = Q_{jk} P_{jk} \qquad j,k = 1,7$$

The generic participation factor ρ_{jk} gives an index of the participation of the j_{th} state to the k_{th} modal shape [15], [16] and so, for each eigenvalue of the above linearized state matrix it is possible to identify the "dominant" state, the one most heavily contributing to the relative modal shape. A modal shape may be participated by more than one state: a dominant and some co-dominant ones. Finally, by the numerical integration of the motion equations system (1) starting from an initial state near to a steady state solution, it is possible to plot the transient behavior until the equilibrium condition and evaluate the attractiveness of such solution.

III. Theoretical Results

As described above, the procedure has been applied on 3 vehicles, based on different traction schemes (RWD, FWD and 4WD), sharing all geometrical and inertial parameters, suspension stiffnesses, aerodynamic characteristics and tires performances. In Figs. 2 the understeer characteristics and sideslip curves for the three vehicles are reported: the considered maneuver is a constant radius (100 m) curve. Each point on the curves corresponds to a steady state equilibrium characterized by 7 eigenvalues and 7 eigenvectors.

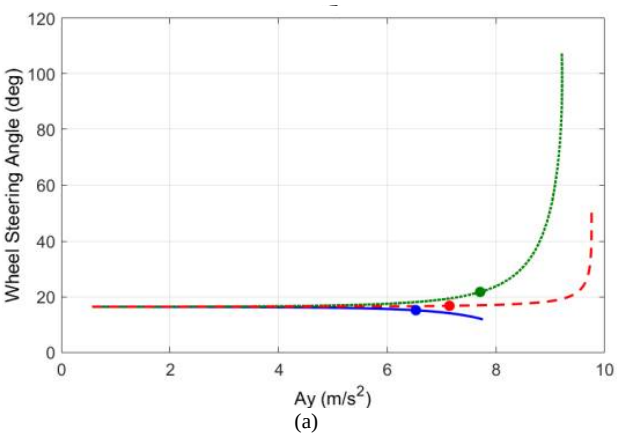

(a)

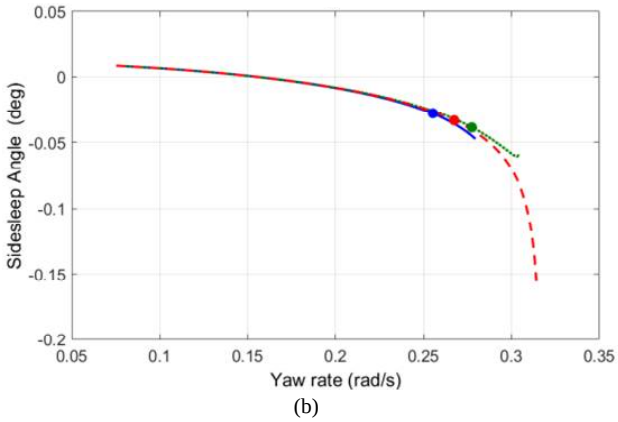

(b)

Figs. 2. Constant Radius (100 m) steering pad maneuver for three vehicles sharing all geometric and inertial parameters, equipped with open differentials, in the case of: Rear wheel drive (blue continuous line), Front wheel drive (green dotted line) and Four-Wheel drive (red dashed line). (a) Understeer characteristics; (b) Sideslip curve

By analyzing the eigenvector matrix in each point of the above curves, it is possible to evaluate the participation of each state in each modal shape.

Moving from left to right, the first points on the curves corresponding to low A_y and r values (i.e. low engine torque) are characterized by a complete separation among the three body motions (U, V and r) and the four tires motions (ω_{ij}). In other words, there are three modal shapes dominated exclusively by one or more car states and other four modal shapes each one dominated by a single tire state. Moving along the curves (i.e. increasing engine torque) such separation disappears at the "coupling points" (marked by a circle) when a driving tire state begins to participate in a modal shape dominated by a car state. From this point until the last one (i.e. the instability beginning), the coupling between the seven motions in the modal shapes increases.

The position of the coupling points on the curves allows observing that the extension of the separation zone grows up passing from a RWD to a 4WD and from a 4WD to a FWD vehicle. Moreover, in the case of a RWD vehicle the tire motion that begins to participate in a modal shape dominated by a car motion is the outer driving tire motion (ω_{22}), while for both 4WD and FWD vehicles it is the inner driving tire one (ω_{11}). Table I reports the seven eigenvalues at the instability beginning with the indication of the motions (i.e. the states) participating to the corresponding modal shape. The first state is the dominant and the other ones follow in order of participation. Once reached the instability threshold, results show that the motion equations are always coupled and, in particular, from the "coupling point" until the instability, one or more-wheel motions participate to the modal shape dominated by a car motion. Moreover, at the instability threshold the unstable eigenvalues are always a complex conjugate pair: this means that instability manifests itself as an undamped vibration.

These considerations suggest the possibility to use wheel speed sensor signals to find a precursor of instability in order to activate a Vehicle Dynamics Control logic. However, all the studied traction schemes show an arising low frequency component in the inner driving wheel angular velocity signal that could be treated as an instability precursor: in particular, ω_{21} for Rear-Wheel-Drive and ω_{11} for both Front and Four-Wheel-Drive. To better clarify the possibility to use wheel angular speed signals as precursor of vehicle's instability, Figs. 3 and 4 report the eigenvalues of the three modal shapes dominated by the three car states U, V and r, as a function of the lateral acceleration A_y, for the three analyzed traction schemes and for two constant radius maneuvers: 40 m, Figs. 3, and 100 m, Figs. 4. Real eigenvalues are highlighted in blue and complex conjugate pair ones in red. In each case, the arising of a low and rapidly increasing frequency component in a body motion constitutes a precursor of the incoming instability: in a RWD vehicle a very low frequency appears in the longitudinal motion U (Figs. 3(a) and 4(a)), in a FWD one a low frequency component (about 1 Hz) appears in the yaw motion r (Figs. 3(b) and 4(b)) and the same happens in a 4WD vehicle with a lower frequency about 0.5 Hz (Figs. 3(c) and 4(c)). As defined above, these unstable motions are participated by one tire motion at least: for example, with reference to the constant radius 100 m maneuver (Table I), ω_{21} participates in RWD vehicle motions, ω_{11} in the FWD vehicle motions and both ω_{11} and ω_{22} in the 4WD vehicle motions. Therefore, the four-wheel speed sensors, always mandatory present in cars, are able to sense such a low frequency in order to activate the control logic. Figs. 5, 6 and 7 show the transient behavior up to the equilibrium for the three examined vehicle schemes. In each figure two families of time histories are reported for each scheme corresponding to two operating points: the first one before the coupling point (low A_y value, i.e. very stable operating point) and the second one in the neighborhood of the instability beginning. These time histories have been obtained by numerically integrating the motion equation system (eq. 1) starting from a state condition near the equilibrium (i.e. by adopting the small perturbation method). It is necessary to consider that system (1) should not be used for transitory analysis and the achieved results allow only qualitative considerations. In the three figures the blue lines refer to very stable conditions: in the time histories of the seven states and in the 3D plot of the car states, no oscillating behaviors can be seen (the equilibrium point appears to be a "node") [17], [18].

The red lines refer to operating points near the instability: in each curve is evident the presence of a damped oscillation at low frequencies for all the three traction schemes, with the RWD frequency lower than the FWD and 4WD ones. In the 3D plot, the equilibrium point appears to be a "focus". The damped vibrations are quite evident in the time histories of V and r car motions, while they are less evident (but anyway appreciable) in the time histories of the wheel speeds.

TABLE I
STATE MATRIX EIGENVALUES CORRESPONDING TO THE LAST POINTS ON THE CURVES OF Fig. 2 (I.E. THE FIRST UNSTABLE SOLUTION), WITH THE INDICATION OF THE STATE(S) PARTICIPATING TO THE CORRESPONDING MODAL SHAPE

	Eigenvalues & Modal shapes						
	1	2	3	4	5	6	7
RWD	0.05 - 0.32i	0.05+ 0.32i	-4.86	-31.44	-31.72	-52.57	-54.27
	(U, r, V, ω_{21})	(U, r, V, ω_{21})	(V, r)	(ω_{11}, ω_{21})	(ω_{21}, ω_{11})	(ω_{12}, ω_{22})	(ω_{22}, ω_{12})
FWD	0.02 - 5.85i	0.02+ 5.85i	-0.02	-3.04	-19.09	-39.28	-42.39
	(r, ω_{11}, V)	(r, ω_{11}, V)	(U)	(ω_{11}, V, r)	(ω_{21})	(ω_{22})	(ω_{12})
4WD	0.03 - 2.40i	0.03 + 2.40i	-0.03	-1.82	-7.39	-35.15	-38.63
	(r, ω_{11}, V)	(r, ω_{11}, V)	(U, ω_{11}, r, ω_{22})	(ω_{11}, r, V, ω_{22})	(ω_{21})	(ω_{12})	(ω_{22})

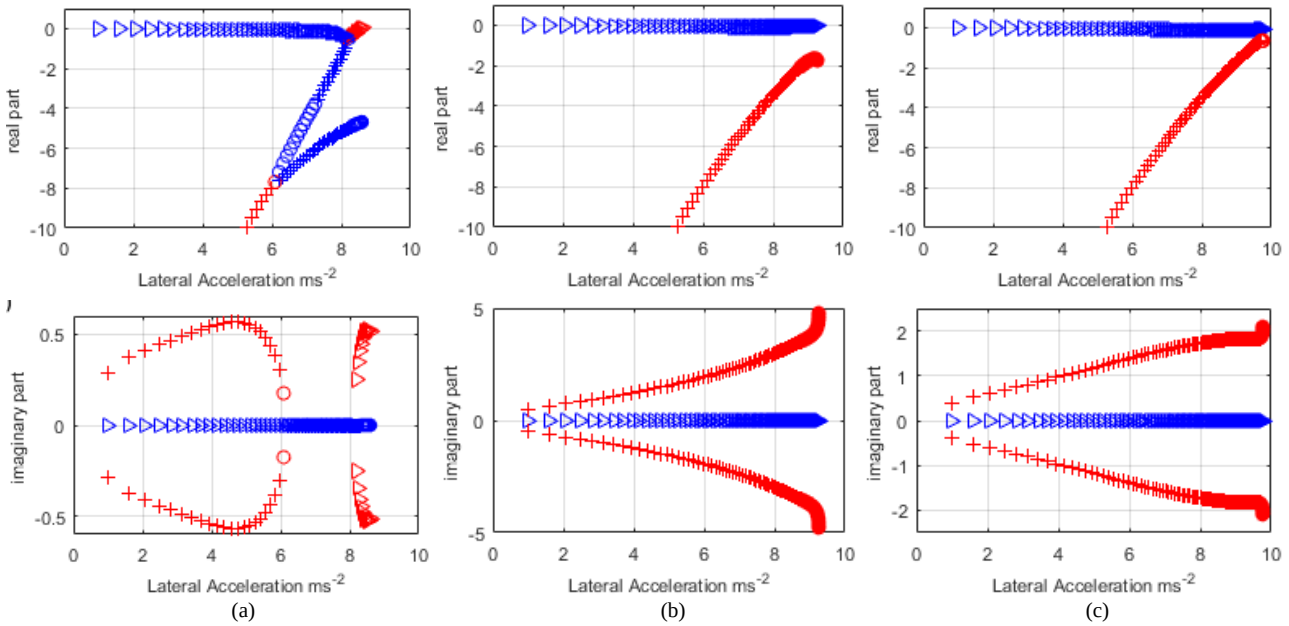

Figs. 3. Eigenvalues of the modes dominated by U (>), V(+) and r (o) vs. lateral acceleration for a vehicle running a 40 m curve: (a) Rear drive, (b) Front drive and (c) Four-wheel drive

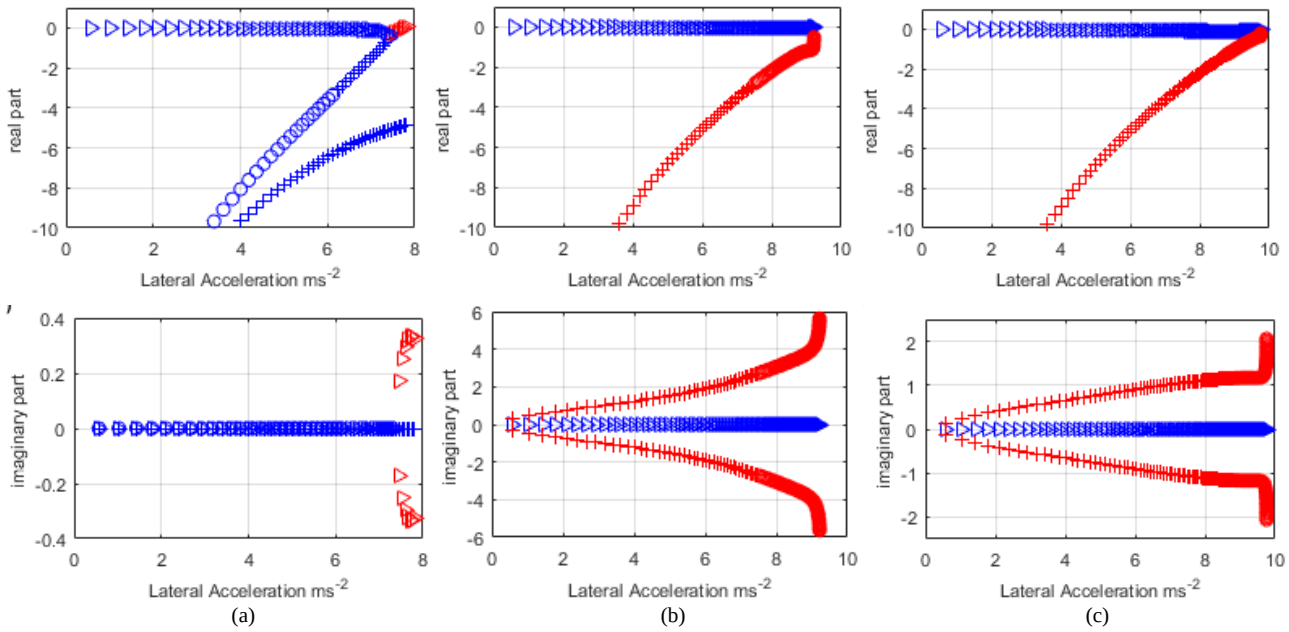

Figs. 4. Eigenvalues of the modes dominated by U (>), V(+) and r (o) vs. lateral acceleration for a vehicle running a 100 m curve: (a) Rear drive, (b) Front drive and (c) Four-wheel drive

In Figs. 5, such vibration is appreciable also in the time histories of the four-wheel speeds and it could be detected by sensors and used as precursor.

In Figures 6 such vibration is appreciable in the time history of the inner driving tire (ω_{11}) wheel speed: also in this case a sensor on this tire could activate a stability control logic.

In Figs. 7, such vibration is appreciable in the time histories of the inner driving tires (ω_{11} and ω_{21}) wheel speeds. Signals from sensors on these wheels could activate the stability control logic.

III.1. Tests in Simulation

In order to have a first validation of the proposed idea in simulation environment, three tests have been performed using CarSim 7, a commercial software widely adopted by car manufacturers. This simulation software allows creating very detailed models of vehicles, engines, drivers, roads and some testing maneuvers can be performed. It offers also the possibility to choose from an extensive library of predefined templates and proceed to customize the test by changing only the parameters of interest.

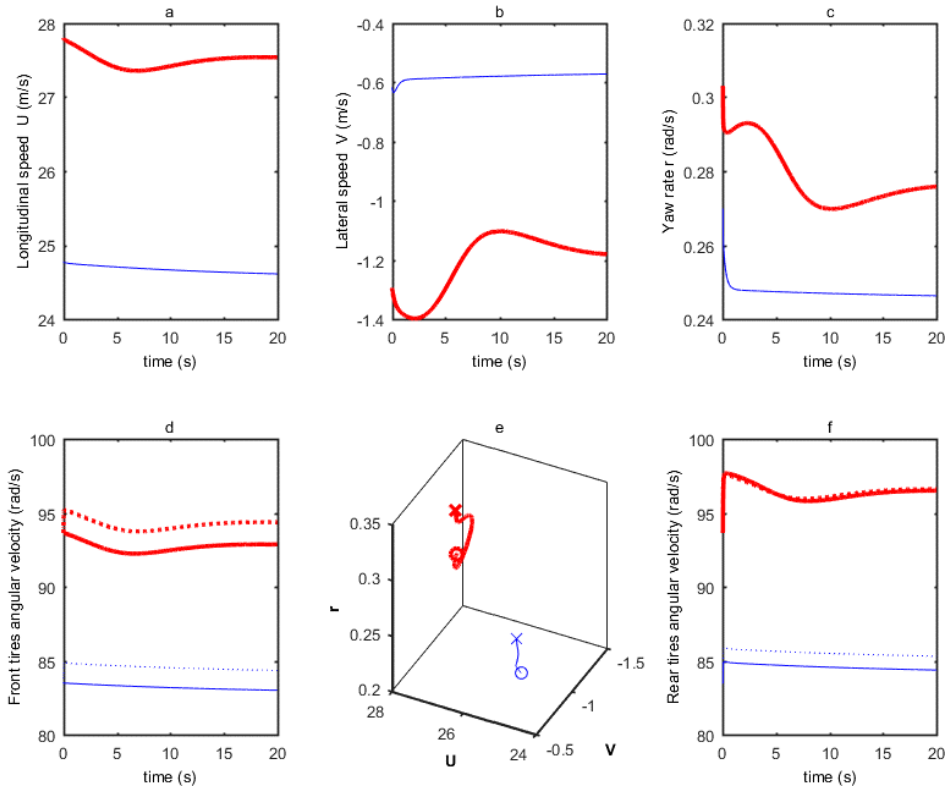

Figs. 5. Rear Drive vehicle: Small Perturbation of two equilibrium points: A_y=6 ms^{-2} (blue thin curves) and A_y=7.5 ms^{-2} (red thick curves). The Time history refers to: a) Longitudinal speed U; b) Lateral speed V; c) Yaw rate r; d) Front wheels speed ω_{11} (solid line), ω_{12} (dashed line); e) Phase trajectories in the space U,V,r ("x" starting point, "o" equilibrium point), f) Rear wheels speed ω_{21} (solid line) , ω_{22} (dashed line)

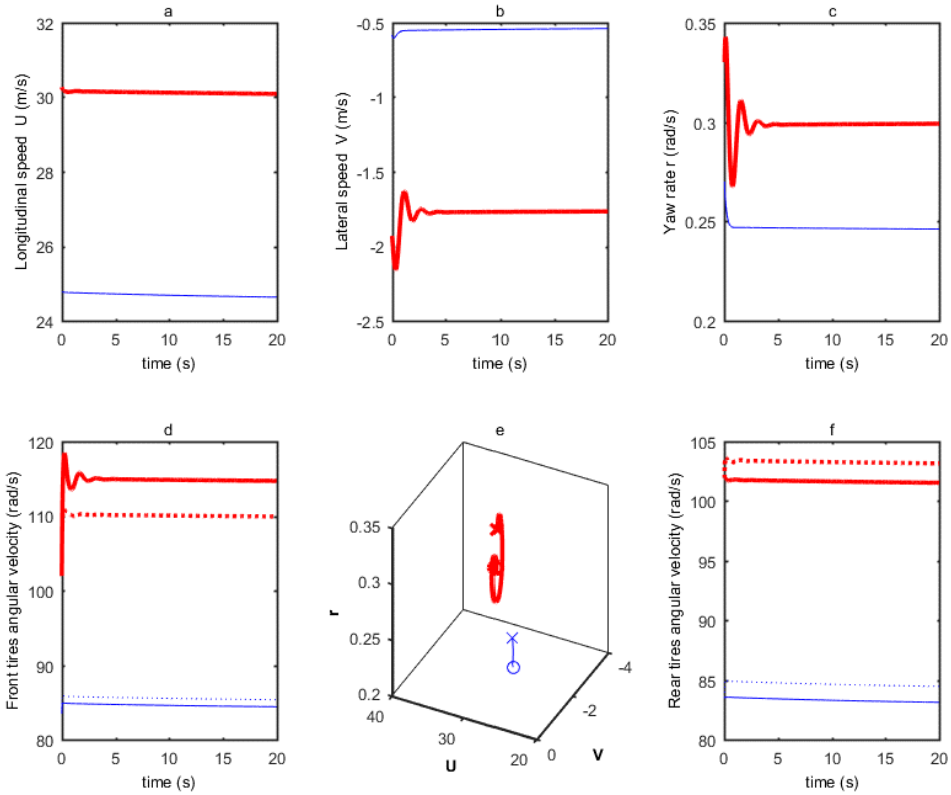

Figs. 6. Front Drive vehicle: Small Perturbation of two equilibrium points: A_y = 6 ms^{-2} (blue thin curves) and A_y = 9 ms^{-2} (red thick curves). The Time histories refer to: a) Longitudinal speed U; b) Lateral speed V; c) Yaw rate r; d) Front wheels speed ω11 (solid line), ω12 (dashed line); e) Phase trajectories in the space U,V,r (x starting point, o equilibrium point); f) Rear wheels speed ω21(solid line) , ω22 (dashed line)

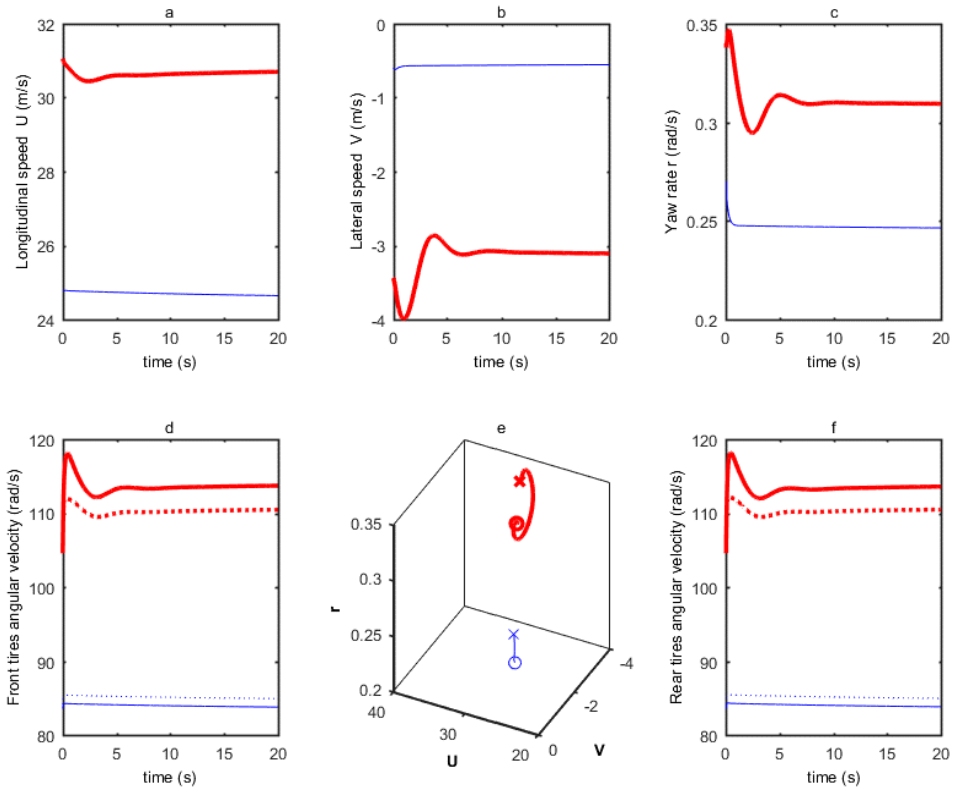

Figs. 7. Four Wheel Drive vehicle: Small Perturbation of two equilibrium points: $A_y = 6\ ms^{-2}$ (blue thin curves) and $A_y = 9.5\ ms^{-2}$ (red thick curves). The Time histories refer to: a) Longitudinal speed U; b) Lateral speed V; c) Yaw rate r; d) Front wheels speed ω_{11} (solid line), ω_{12} (dashed line); d) Phase trajectories in the space U,V,r (x starting point, o equilibrium point); f) Rear wheels speed ω_{21} (solid line), ω_{22} (dashed line)

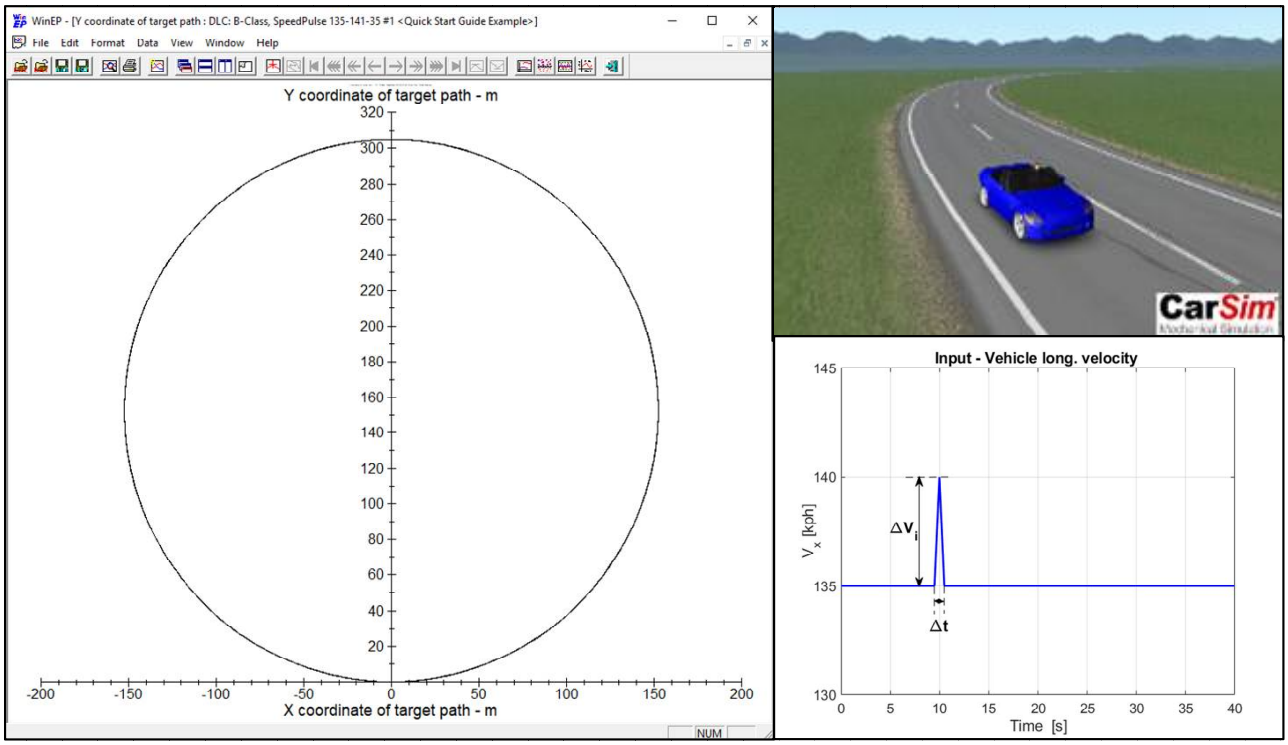

Fig. 8. Circle manoeuvre in CarSim environment: a pulse speed profile used in the performed tests

The vehicle model selected in CarSim to carry on the simulation tests is the "B-Class, Sport Car" equipped by a 150kW 6-speed engine. All the characteristics provided by the CarSim library model have been kept constant except for the traction scheme configuration for which three different solutions have been considered: Rear Drive open (free) differential, Front Drive open differential and Four-Wheel Drive open differentials. The geometrical, inertial and compliance data of such vehicle and tire-road characteristics, are surely different from the ones used to solve the mathematical model (eq. (1)), but the simulated tests only aim to investigate about the qualitative tendencies and behaviors.

In the simulations (Fig. 8), the three vehicle schemes travel on a circular (500 ft, about 152 m) smooth road at a constant speed of 135 km/h. The tire-road friction is constant and equal to 1. To alter the steady state equilibrium, several perturbations as target speed pulse are imposed (in 1 s), starting from the constant speed V = 135 km/h. To highlight the behavior in small perturbations' conditions, different pulse amplitudes have been performed with the aim to show what happens in the instants immediately preceding a possible instability (that can be different because of the different traction scheme). Three speed pulse tests have been performed, at different amplitudes, with the aim of investigating the in-curve behaviour (around incipient vehicle instability conditions) by monitoring wheel speed signals.

As shown in Table II, different velocities have been considered. Because of the different drivelines, different speed amplitudes must be reached to cause the instability: in all the cases, a pulse of 1s duration is expected to keep small perturbations conditions.

TABLE II
STEERING PAD PERFORMED IN CARSIM ENVIRONMENT: TESTS DEFINITION

Traction scheme	Speed pulse – Amplitude (km/h)	Time (s)
RWD	$\Delta V_1 = 5$, $\Delta V_2 = 8$, $\Delta V_3 = 11$	$\Delta t = 1$
FWD	$\Delta V_1 = 5$, $\Delta V_2 = 10$, $\Delta V_3 = 15$	$\Delta t = 1$
4WD	$\Delta V_1 = 5$, $\Delta V_2 = 10$, $\Delta V_3 = 15$	$\Delta t = 1$

Figs. 9, 10 and 11 report the wheel speeds outputs provided by CarSim simulations in all the considered traction schemes (RWD, FWD and 4WD): the peak in the pulse in speed occurs 10 seconds after the starting of simulation. In the wheel speed time histories, a damped low frequency oscillation is clearly recognizable in the inner driving tire (rear left for RWD, front left both for FWD and 4WD) in all the transient phases following the perturbations. Such damped oscillation is also appreciable in all the other wheels and in particular in the inner non-driving tire. The step in the pulse amplitude is different in the 3 considered traction schemes: being RWD vehicle less stable if compared with other schemes, a smaller perturbation (ΔV_3 = 11 km/h) is sufficient to get the instability, while being FWD the most stable also a great perturbation (ΔV_3 = 15 km/h) is not sufficient to reach the instability.

In particular, Fig. 12 shows the comparison among the inner drive (rear left for RWD, front left both for FWD and 4WD) wheel speeds signals for the 3 different amplitudes of the speed pulse: the amplitude of the damped oscillations (proposed as instability precursor) increases as the vehicle approaches to the instability. Such oscillations are easily detectable from wheel speed encoders that are mandatory on board.

It is necessary to highlight that in the 4WD case, the instability is not reached: the vehicle is able to recover the stability. Similar considerations can derive from the analysis of the vehicle CoG trajectories. In Fig. 13, it is evident the total spin instability of the RWD vehicle because of a small pulse perturbation amplitude, an understeer instability for the FWD one and, finally, the ability to recover the stability characterising the 4WD vehicle, even in case of a great pulse perturbation amplitude.

Again, with reference to above simulated tests, Figs. 14, 15 and 16 show the time histories of the vehicle body motions: vehicle accelerations (longitudinal and lateral) and velocities (longitudinal, lateral and yaw rate). Before the instability occurs, for all the considered traction schemes, the longitudinal and lateral accelerations, easily sensed by a normal driver, show very small amplitude damped oscillation, even for the greater value of the speed pulse amplitude.

Therefore, these signals, even if available, cannot be assumed as valid precursors of instability (only in the FWD scheme, a damped oscillation with small amplitude is recognizable). Similar considerations can be made for vehicle velocities. The yaw rate, instead, shows appreciable amplitude of the damped oscillation. The amplitudes of these oscillations increase more and more approaching the instability in RWD traction scheme. Therefore, in this case, it could be considered as valid precursor of instability. In the other two traction schemes (FWD and 4WD), the yaw rate does not show a univocal trend in the damped oscillation amplitude after the imposed perturbation. In particular, as concerns FWD vehicle, showing an understeering behaviour (Fig. 13), the above amplitude decreases more and more approaching to the instability. While, in 4WD vehicle case, showing a stable behaviour (able to recover the trajectory after the perturbation), the damped oscillation amplitude does not show a univocal trend.

The above considerations suggest the use of wheel speed encoder signals as precursors of instability and advise against the use of yaw rate signal to the same aim. Moreover, yaw rate sensors are not available on-board of common passenger cars.

III.2. Tests on Road

In order to evaluate the possibility to adopt the tire speed signals as instability precursors it is necessary to verify the "measurability" of small frequency oscillations in such speed signals with the available sensors.

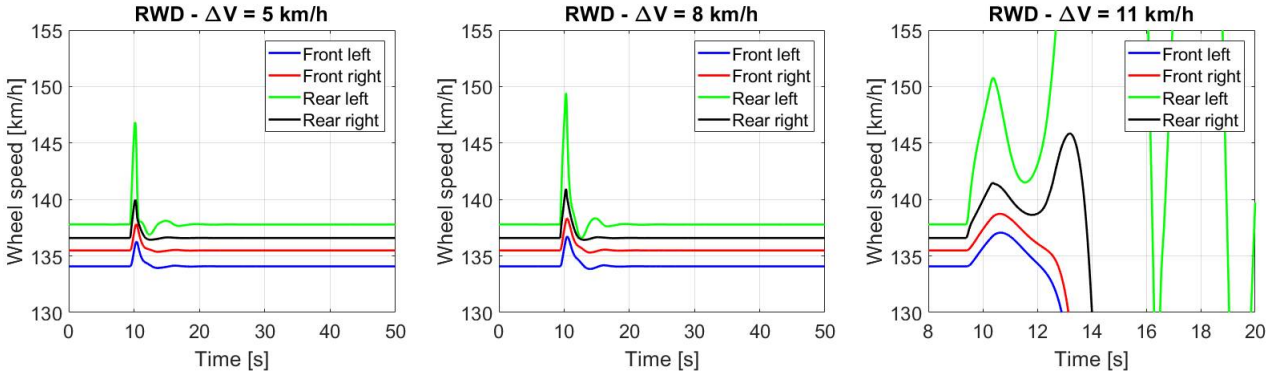

Fig. 9. Speed pulse for Rear-Wheel-Drive scheme, simulated test in CarSim: low frequency vibrations in wheel speed signals at t=10s. Variations of speed pulse amplitude up to the lateral instability. It is observable inner tire plays a crucial role

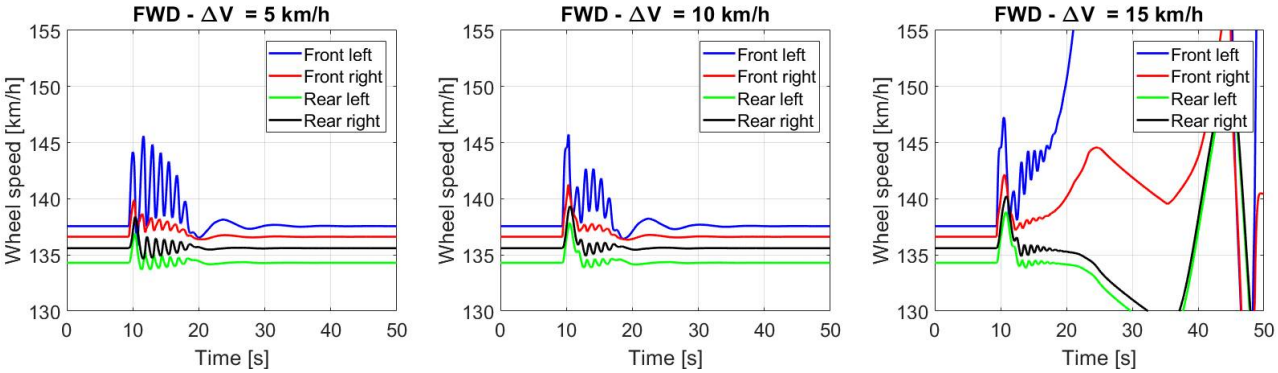

Fig. 10. Speed pulse for Front-Wheel-Drive scheme, simulated tests in CarSim: low frequency vibrations in wheel speed signals at t=9.94 s. Variations of speed pulse amplitude up to the lateral instability. It is observable inner tire plays a crucial role

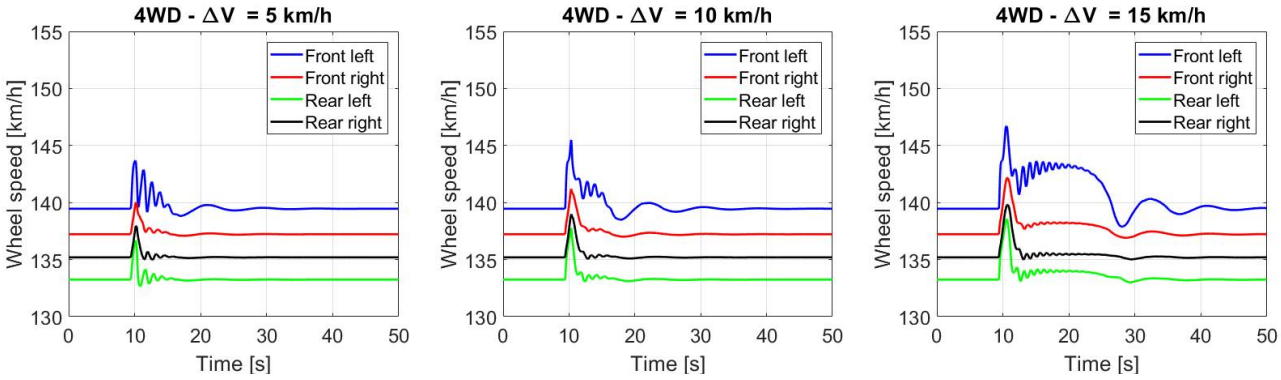

Fig. 11. Speed pulse for 4-Wheel-Drive, simulated test performed in CarSim: low frequency vibrations in wheel speed signals at t=30s. Variations of speed pulse amplitude up to the lateral instability. It is observable inner tire at rear axle plays a crucial role

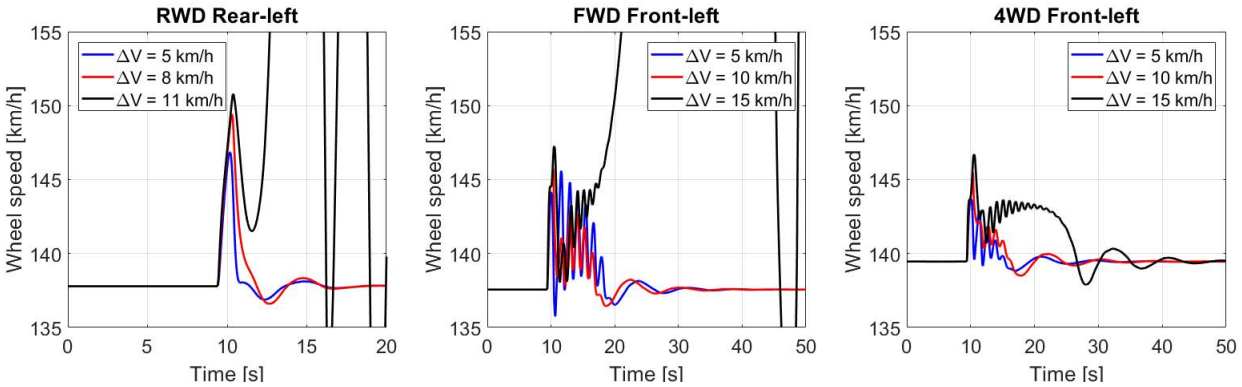

Fig. 12. Inner drive wheel speed in the simulation tests performed in CarSim at different pulse amplitude values

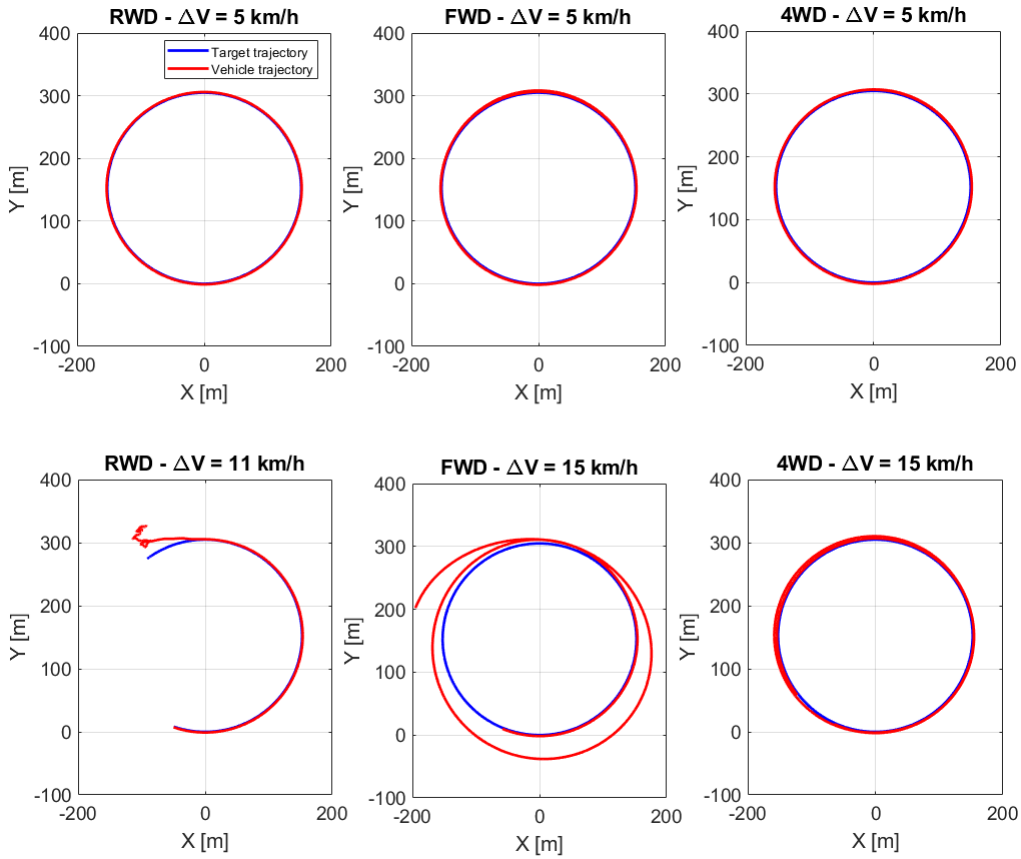

Fig. 13. Simulated tests performed in CarSim: CoG vehicle trajectory

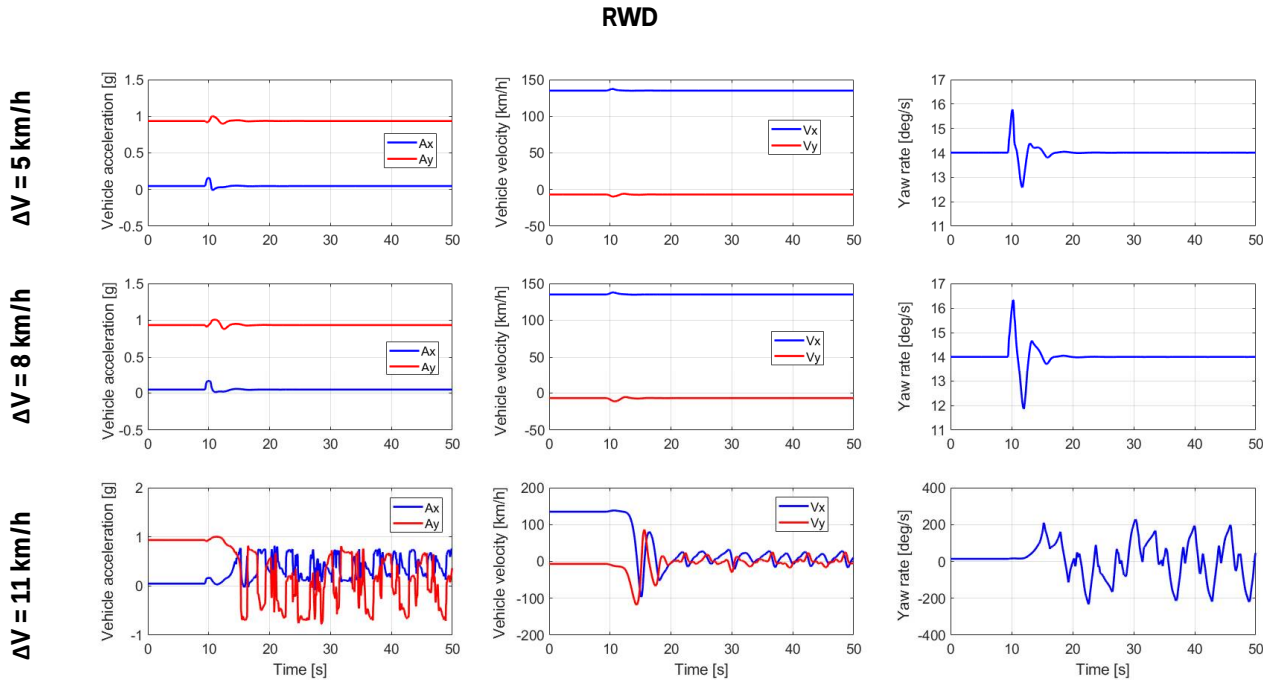

Fig. 14. Simulated tests performed in CarSim: vehicle accelerations (longitudinal and lateral) and velocities (longitudinal, lateral and yaw rate) for the Rear-Wheel-Drive traction scheme

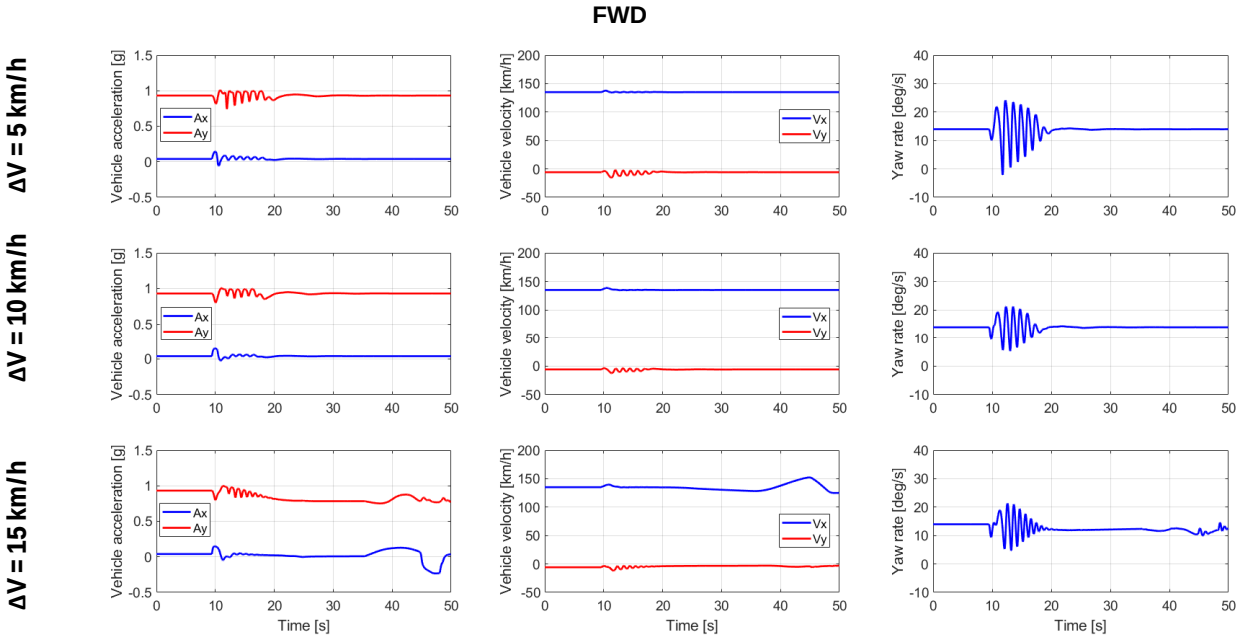

Fig. 15. Simulated test performed in CarSim: Longitudinal and lateral accelerations and velocities for the Front-Wheel-Drive traction scheme

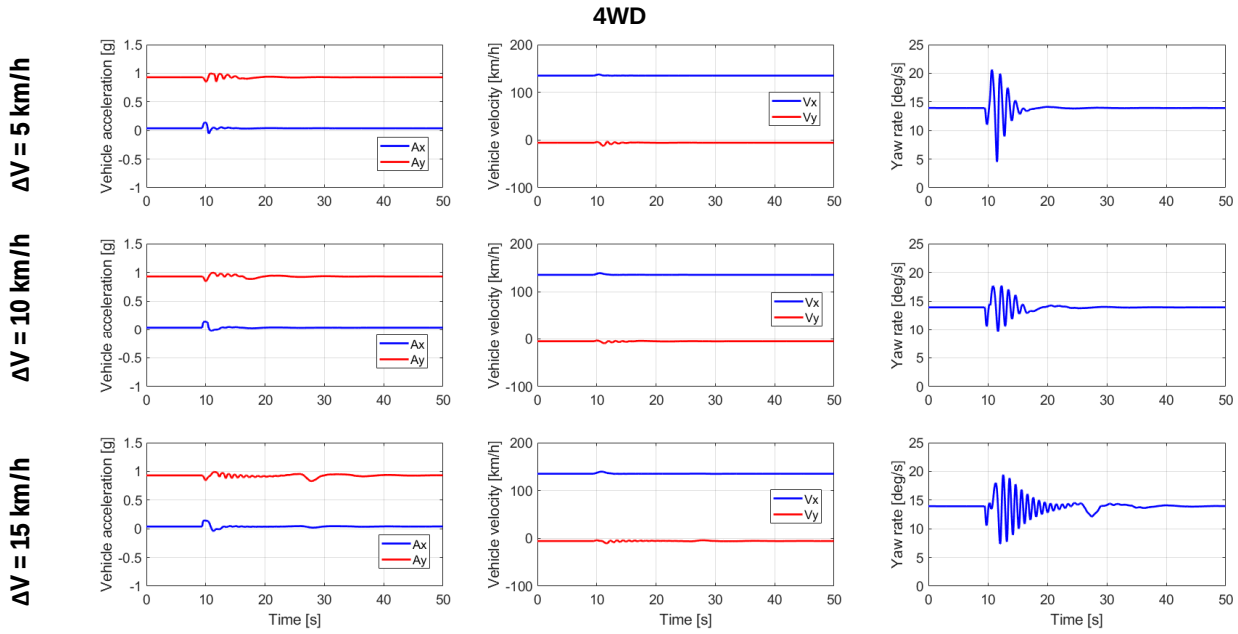

Fig. 16. Simulated test performed in CarSim: Longitudinal and lateral accelerations and velocities for the Four-Wheel-Drive traction scheme

Figures below show the output provided by two instrumented vehicles during some outdoor test maneuvers. The vehicles are GT cars and the presented outdoor tests were not aimed to validate the proposed precursors analysis.

Two experimental acquisitions will be shown:

1. Steering-pad (RWD traction scheme);
2. Chicane limit maneuver (FWD traction scheme).

It is necessary to start from a steering-pad maneuver (Figs. 17), consistent with the proposed study of this paper. The vehicle, in this case, is RWD and the steering-pad is a right curve maneuver.

By analyzing the time histories, it can be noted that in the range 18÷22 seconds a low frequency phenomenon appears in the lateral acceleration signal. Such low frequency is perceived by the expert test driver who firstly reduces speed and then let off completely the throttle (see the longitudinal velocity time histories). By analyzing the velocity signals coming from the encoders (in this road test the wheel angular velocity is converted in longitudinal velocity by multiplying the signals by a nominal rolling radius), it is possible to note, around the second 19, the onset of a vibration in the outer rear tire signal.

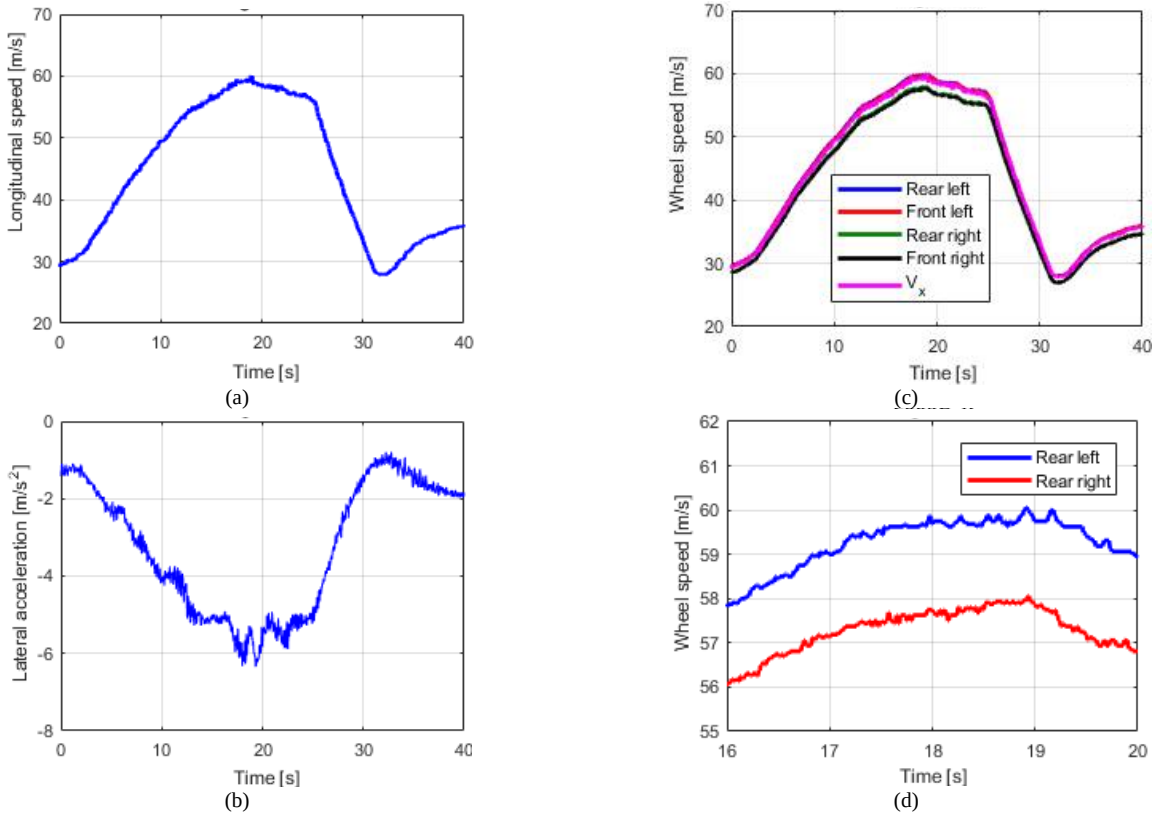

Figs. 17. Road Test: a) longitudinal speed, b) lateral acceleration, c) wheel centres velocity, d) zoom on the driving wheel centres velocity (the upper blue line refers to the outer tire, the lower red to the inner one)

Such vibration could constitute the precursor of instability that will be able to activate a stability control logic. The second test consists in a chicane limit maneuver performed by a FWD vehicle in high grip conditions (Monza circuit dry, Fig. 18). By analyzing the velocity signals coming out from the wheel speed encoders (Fig. 19), it is possible to observe low frequency damped oscillations, most evident in the inner front wheel signals.

In Fig. 18, the three curves of the considered chicane are analyzed. During the first left curve, the low frequency oscillation appears clearly in the left front wheel (the inner one), around the second four.

Fig. 18. The chicane layout of the chicane travelled during the manoeuvre

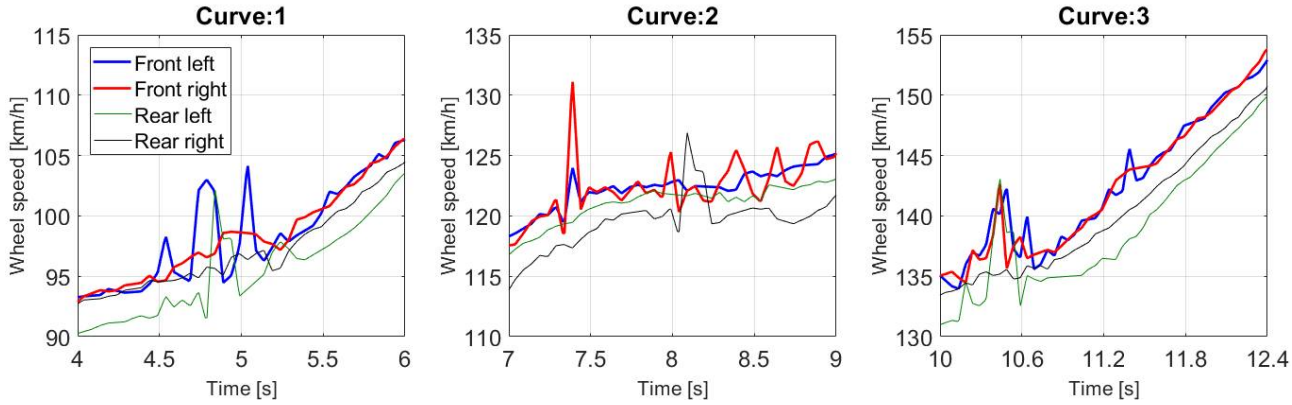

Fig. 19. Chicane limit manoeuvre: low frequency vibrations in wheel peripherical speed signals

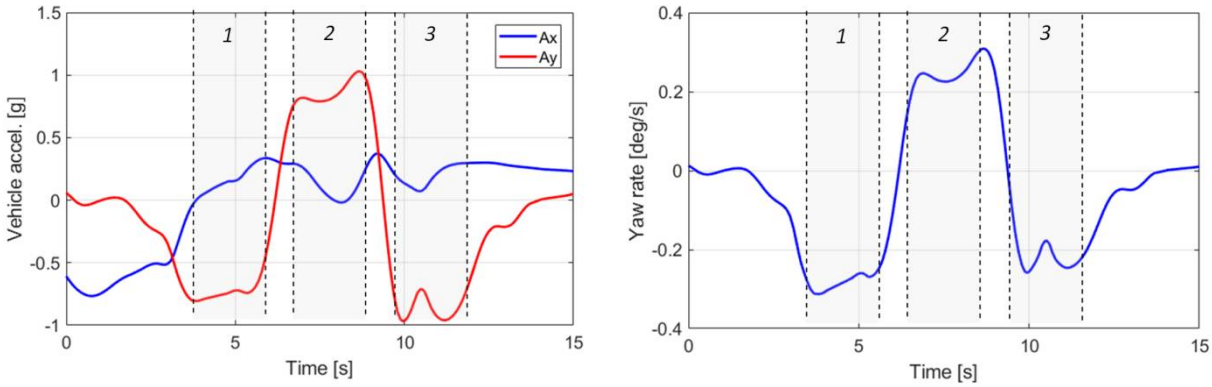

Fig. 20. Chicane limit manoeuvre: Longitudinal and lateral Vehicle CoG accelerations and yaw rate, with an indication of the 3 curves

The incipient instability is clearly demonstrated by the low frequency oscillation at the second 10 in all the wheel sensor speed signals in Fig. 19. Moreover, once the stability has been recovered by the test driver, low frequency oscillation appears again in the left front wheel (the inner one) around the second 11.5. When the vehicle is travelling the second right curve, it is possible to highlight how these low frequency moves to the right front wheel (the inner one, in this other case), around the second 7. Finally, in the third left curve, the expert driver, perceiving an incipient instability, has decreased both longitudinal and lateral accelerations (around second 10 in Fig. 20) by reducing throttle and steering angle. Once again, the analysis of Figs. 19 and 20 shows that the low frequency oscillations are recognizable only in the wheel speed signals, as a confirmation of the mentioned approach. The higher amplitudes are recognizable for front wheel because of the Front-Wheel-Drive traction scheme.

IV. Conclusion

A theoretical approach to the definition of instability precursors for a vehicle running in curve with constant velocity has been presented. The precursors have been individuated as low frequency oscillations in the time histories relative to the seven vehicle states: longitudinal and lateral velocities, yaw rate and the four-wheel speeds. The application of this approach to a study on a modern car, tested both in simulation and on-road tests, has shown that the individuated precursors are always well evident and coherent in the wheel speed signals but not in the car motions ones: longitudinal, lateral accelerations and yaw rate. The analysis of the theoretical, numerical and experimental tests has confirmed that the wheel speed signals can be adopted has valid instability precursors with the aim to apply stability control logics. Therefore, this approach is suitable for all modern vehicles, which are always equipped with wheel speed sensors (mandatory).

References

[1] Rajamani R. *Vehicle Dynamics and Control, Springer*, USA,2006.

[2] Guiggiani M. *Vehicle Dynamics*. Italia: Città studi Edizioni, 2007 (In Italian).

[3] Gillespie TD. *Fundamentals of vehicle dynamics*, Society of Automotive Engineering, Warrendale, 1992.

[4] Pacejka HB. *Tire and vehicle dynamics*. 3d ed. Oxford, UK: Elsevier; 2012.

[5] M. Boisvert, P. Micheau. Estimators of wheel slip for electric vehicles using torque and encoder measurements. *Mechanical Systems and Signal Processing*, vol. 76–77, pp 665-676, 2016. https://doi.org/10.1016/j.ymssp.2016.02.017

[6] Jun Ni, Jibin Hu. Dynamics control of autonomous vehicle at driving limits and experiment on an autonomous formula racing car. *Mechanical Systems and Signal Processing*, vol. 90, pp. 154-174, 2017. https://doi.org/10.1016/j.ymssp.2016.12.017

[7] Takahashi J, Yamakado M, Saito S, Yokoyama A. A hybrid stability-control system: combining direct-yaw-moment control and G-Vectoring Control. *Veh Sys Dyn*. 2012; 50(6): 847-899.

[8] Xiao H, Chen W, Zhou HH, Zu JW. Integrated control of active suspension system and electronic stability program using hierarchical control stategy: theory and experiments. *Veh Sys Dyn.* 2011; 49 (1-2): 381-397.

[9] Poussot-Vassal C, Sename O, Dugard L, Savaresi M. Vehicle dynamic stability improvements through gain-scheduled steering and braking control. *Veh Sys Dyn.* 2011; 49(19):1597-1621.

[10] Canale M, Fagiano L. Comparing rear wheel steering and rear active differential approach to vehicle yaw control. *Vhe Sys Dyn.* 2010; 45(5):529-546.

[11] Russo R, Terzo M, Timpone F. Software-in-the-loop development and validation of a cornering brake control logic. *Veh Syst Dyn.* (Netherlands) 2007;45(2):149–163.

[12] L. De Novellis, A. Sorniotti, P. Gruber. Driving modes for designing the cornering response of fully electric vehicles with multiple motors. *Mechanical Systems and Signal Processing*, vol. 64–65, pp. 1-15, 2015. https://doi.org/10.1016/j.ymssp.2015.03.024

[13] B. Lenzo, G. De Filippis, A. M. Dizqah, A. Sorniotti, P. Gruber, S. Fallah and W. De Nijs. Torque Distribution Strategies for Energy-Efficient Electric Vehicles With Multiple Drivetrains. *Journal of Dynamic Systems, Measurement and Control, Transactions of the ASME*, vol. 139, issue 12, Article number 121004, 2017. Paper No: DS-16-1402. https://doi.org/10.1115/1.4037003

[14] R. S. Sharp, The lateral dynamics of motorcycles and bicycles, *Veh Syst Dyn.* (Netherlands) 1985; 14: 265-283.

[15] Meirovitch L. *Dynamics and control of structures*, New York: John Wiley & Sons; 1990.

[16] Aboul-Ela M. E., Sallam A. A., McCalley J. D., Fouad A. A., Damping controller design for power system oscillations using global signals. *IEEE Trans. on Power Systems* 1996; 11 (2): 767-773.

[17] Khalil HK. *Nonlinear Systems*. 3d ed. Upper Saddle River, NJ USA: Prentice-Hall;2012.

[18] Farroni F et al., A combined use of phase plane and handling diagram method to study the influence of tyre and vehicle

characteristics on stability. *Veh Syst Dyn*. (Netherlands) 2013; 51(8): 1265-1285.

Authors' information

Department of Industrial Engineering, University of Naples Federico II, via Claudio 21, Naples, Italy.

Giandomenico Di Massa is professor of mechanics of machinery at the University of Naples Federico **II**, Italy.
His theoretical and experimental activities regards: motorcycle dynamics, shimmy phenomenon, modelling and simulation of mechanical systems, mechanical vibrations, analytical dynamics, seismic insulation.

S. R. Pastore received his M.Sc. degree in Mechanical Engineering in 2015 at the University of Naples "Federico II", where he is currently a Ph.D. student in Industrial Engineering department. His research work is mainly focused on the tyre and vehicle control systems modeling and experimental activites for vehicle, tyre and rubber compound characterizations in both dry and wet conditions.

Riccardo Russo was born in Sarno, Salerno (Italy) on 1957. He received the M.Sc. degree in Mechanical Engineering at the University of Naples Federico II in 1984. He is full professor in Applied Mechanics. He is author of more than 100 articles in several fields such as Lubrication, Dynamics of rotors, Vehicle Dynamics, Robotics, Control of mechanical systems and Mechanical measurements. He is member of the Italian Association of Theoretical and Applied Mechanics (AIMETA) and of IFToMM Italy.
E-mail: riccardo.russo@unina.it

F. Timpone (Naples, 5th of September 1974) received the M.Sc. degree in Mechanical Engineering in 1999 and the Ph.D. degree in Thermomechanical System Engineering in 2004 both from the University of Naples "Federico II". He is Associate Professor of Applied Mechanics and Vehicle Dynamics at the University of Naples "Federico II" and his research interests include the dynamics and the control of mechanical systems.

